Evidence for a wide and gently dipping Main Himalayan Thrust in western Bhutan

Romain Le Roux-Mallouf, Vincent Godard, Rodolphe Cattin, Matthieu Ferry, Jampel Gyeltshen, J.F. Ritz, Dowchu Drupka, Valery Guillou, Maurice Arnold, G. Aumaître, et al.

AGU PUBLICATIONS

Geophysical Research Letters

RESEARCH LETTER
10.1002/2015GL063767

Key Points:
- Assessment of denudation rates in Himalayas
- Robust constrain on the location of the flat-ramp transition of the MHT
- Evidence of a strong lateral variation in the MHT geometry

Supporting Information:
- Text S1, Figures S1–S6, and Tables S1–S3

Correspondence to:
R. Cattin,
cattin@gm.univ-montp2.fr

Citation:
Le Roux-Mallouf, R., et al. (2015), Evidence for a wide and gently dipping Main Himalayan Thrust in western Bhutan, *Geophys. Res. Lett.*, *42*, doi:10.1002/2015GL063767.

Received 10 MAR 2015
Accepted 6 APR 2015
Accepted article online 10 APR 2015

Evidence for a wide and gently dipping Main Himalayan Thrust in western Bhutan

Romain Le Roux-Mallouf[1], Vincent Godard[2], Rodolphe Cattin[1], Matthieu Ferry[1], Jampel Gyeltshen[3], Jean-François Ritz[1], Dowchu Drupka[3], Valéry Guillou[2], M. Arnold[2], G. Aumaître[2], D. L. Bourlès[2], and K. Keddadouche[2]

[1]Géosciences Montpellier, CNRS, UMR5243, Université de Montpellier, Montpellier, France, [2]Aix-Marseille Université, CNRS, IRD, Aix-en-Provence, France, [3]Seismology and Geophysics Division, Department of Geology and Mines, Thimphu, Bhutan

Abstract The Main Himalayan Thrust (MHT) is the source of great earthquakes that have been documented along the range. Its geometry is a key parameter that influences accommodation of tectonic loading and earthquake magnitudes along the Himalayan Arc. Although seismic images are available for both the western and the central part of the range, this geometry remains poorly constrained for the Bhutanese Himalayas. Here we address this issue using a ^{10}Be cosmogenic nuclides denudation transect across western Bhutan. We observe a wide low denudation rate domain between 50 km and 110 km from the front followed by a strong northward increase. Using a joint inversion of denudation rates, GPS data, and Holocene uplift rates, we interpret this pattern as a consequence of a flat-ramp transition along the MHT. Compared to central Nepal and Sikkim, this location of the ramp suggests a wider décollement, with implications for greater seismogenic potential of the MHT in western Bhutan.

1. Introduction

The magnitude 7–8 earthquakes occurring along the Himalayan Arc are one of the most dramatic manifestations of the shortening between India and Eurasia [e.g., *Bollinger et al.*, 2014]. Over geological time scales, it is now well established that this frontal deformation has been accommodated along crustal-scale south verging thrust faults including the Main Central Thrust (MCT), the Main Boundary Thrust (MBT), and the Main Frontal Thrust (MFT). These structures strike the entire length of the Himalayan Arc and merge into a common décollement at depth: the Main Himalayan Thrust (MHT) [*Gansser*, 1964]. Over shorter time scales, river terraces observations and GPS measurements in central and eastern Himalaya indicate that the geodetic shortening rate of 15–21 mm/yr is almost entirely accommodated by thrusting on the MFT [e.g., *Lavé and Avouac*, 2000, 2001; *Ader et al.*, 2012; *Burgess et al.*, 2012; *Berthet et al.*, 2014]. The associated interseismic loading is suggested to be released through major earthquakes initiating beneath the Higher Himalayas and propagating southward up to the MFT [*Cattin and Avouac*, 2000]. The geometry of the MHT is thus a key parameter to improve seismic hazard assessment in the region. This geometry is now well established from receiver function images in Garhwal, central and eastern Nepal, and Sikkim [e.g., *Schulte-Pelkum et al.*, 2005; *Nábělek et al.*, 2009; *Acton et al.*, 2011; *Caldwell et al.*, 2013]. However, in other parts of the range—such as Bhutan—it remains poorly constrained. Gravity measurements provide a first-order estimate of the Moho depth beneath Bhutan [*Hammer et al.*, 2013], but, except for the preliminary seismic results of *Acton et al.* [2011] and *Hetényi et al.* [2014], the geometry of the MHT has not been yet directly resolved for this region.

This lack of detailed seismic image leads to contrasting propositions for the geometry of the MHT in Bhutan. *Robert et al.* [2011] use thermokinematic modeling of apatite fission track data to propose a planar MHT with a constant dip angle of 5–7° and no lateral variations, whereas *Coutand et al.* [2014], using a much larger data set with various thermochronometers inferred a more complex geometry including along-strike variations, with a steep frontal ramp and a horizontal section at a depth of 10–15 km that connects to a 30° dipping midcrustal ramp.

In western Bhutan, the geometry proposed by *Coutand et al.* [2014] is partially controlled by the image obtained along the International Deep Profiling of Tibet and the Himalaya (INDEPTH) seismic profiles Tib-1 and Tib-2 within the Yadong-Gulu rift [e.g., *Alsdorf et al.*, 1998a, 1998b; *Hauck et al.*, 1998] (see Figure 1 for location). This structure, associated with one of the largest N-S trending extensional systems crossing the Himalayas and southern Tibet, causes significant changes in the topography and in the depth of the MHT

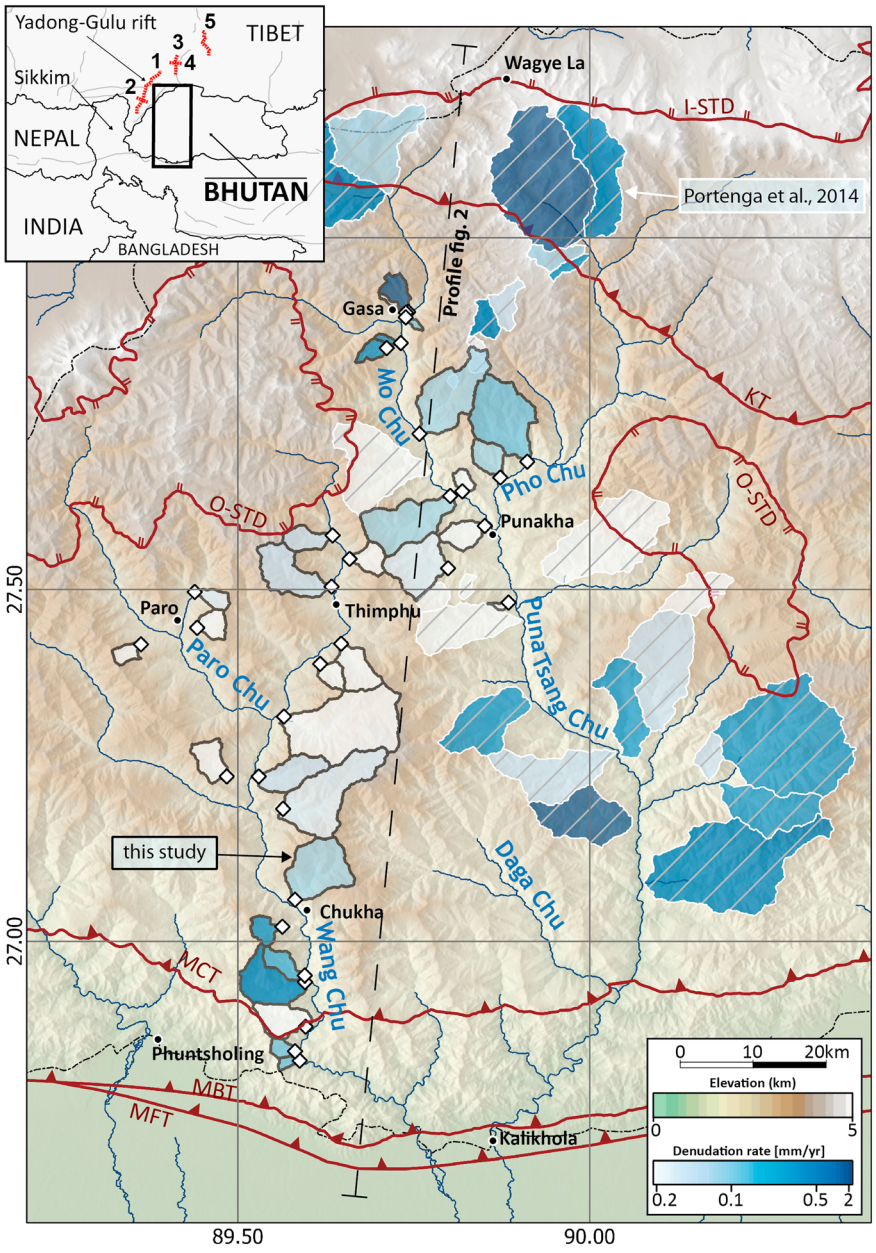

Figure 1. Sampled basins and regional context. Inset shows the location of the study area and International Deep Profiling of Tibet and the Himalaya (INDEPTH) seismic profiles Tib-1 through Tib-5 in red [after *Alsdorf et al.*, 1998a, 1998b; *Hauck et al.*, 1998]. Simplified major faults (grey lines) from *Replumaz and Tapponnier* [2003]. Location of sampled catchments and associated ^{10}Be-derived denudation rates in the western Bhutan Himalayas. Main figure shows the 32 catchments sampled for this study (solid black contours) and catchments sampled by *Portenga et al.* [2014] (white contours with hatching). White diamonds indicate the locations of stream outlets. The black dashed line is the centerline of the 20 km wide swath profile presented in Figure 2. MFT: Main Frontal Thrust; MBT: Main Boundary Thrust; MCT: Main Central Thrust; KT: Kakhtang Thrust; I-STD: Inner South Tibetan Detachment; O-STD: Outer South Tibetan Detachment (structures after *Kellett et al.* [2009] and *Long et al.* [2011]). Additional information on the distribution of precipitation, hillslope angles, and bedrock geology [after *Long et al.*, 2011] is provided in the supporting information (Figure S2).

which is suggested to be displaced along a lateral ramp [*Hauck et al.*, 1998]. Furthermore, receiver function analysis [*Acton et al.*, 2011] as well as gravity measurements [*Hammer et al.*, 2013] also suggest E-W variations in both the Moho and the MHT depths between Nepal and Bhutan.

Over the last decade, several studies relied on cosmogenic nuclides (^{10}Be) concentrations in river sediments to document denudation patterns in the Himalayas [e.g., *Vance et al.*, 2003; *Wobus et al.*, 2005; *Lupker et al.*,

2012; *Godard et al*., 2012, 2014; *Scherler et al*., 2014; *Portenga et al*., 2014]. It has been suggested that such data can provide significant insight into tectonically driven rock uplift and the geometry of related crustal structures [*Wittmann et al*., 2007; *Cyr et al*., 2010; *Gudmundsdottir et al*., 2013]. For example, assuming that the spatial distribution of denudation is mainly controlled by tectonics, *Scherler et al*. [2014] constrain variations in the dip angle of the MHT in the Garhwal Himalayas.

Here following *Scherler et al*. [2014] we use a N-S denudation profile to investigate the geometry of the MHT in western Bhutan (Figure 1). We first present a new data set of denudation rates derived from ^{10}Be concentrations in river sediments that averages surface processes over the 300–20,000 year time scale [*Brown et al*., 1995; *von Blanckenburg*, 2005]. Next, we investigate the geomorphic significance of our data, by analyzing the spatial pattern of denudation across the range. Then, we perform a joint inversion of (1) a combined denudation profile derived from our measurements and those obtained by *Portenga et al*. [2014], (2) an Holocene surface uplift rate on the MFT derived from the study of fluvial terraces in south-central Bhutan [*Berthet et al*., 2014], and (3) a horizontal GPS velocity profile [*Vernant et al*., 2014] to investigate the geometry of the MHT. Finally, our results are compared with findings published by *Robert et al*. [2011] and *Coutand et al*. [2014].

2. Methods

2.1. Sampling Strategy

We use cosmogenic nuclides inventories (^{10}Be) in river sediments [*von Blanckenburg*, 2005] to document the spatial distribution of denudation across western Bhutan. We sampled sands from 32 catchments along a 120 km long north-south profile following the Wang Chu, Paro Chu, Mo Chu, and Pho Chu, from the southern frontal foothills directly north of the MFT, and up to the Higher Himalaya (Figures 1 and 2).

We carefully selected these basins to avoid some of the biases associated with this method. First, we sampled catchments with homogeneous lithologies—on the basis of available geological maps [*Long et al*., 2011]—to limit spatial variations in quartz content in bedrock formations. Second, we selected catchments with no glacial coverage because the input of glacier-derived sediments can significantly complicate the interpretation of ^{10}Be concentrations [*Wittmann et al*., 2007; *Norton et al*., 2010; *Godard et al*., 2012]. Finally, small catchments (<5 km^2) are avoided, as they often do not appropriately account for the contribution of landslides to long-term landscape evolution [*Niemi et al*., 2005; *Yanites et al*., 2009]. A detailed description of our data and analytical methods is provided in the supporting information.

2.2. Inversion Method

Assuming that the observed denudation rates are primarily controlled by the rock uplift pattern across the range [e.g., *Godard et al*., 2014; *Scherler et al*., 2014], our new data set may be interpreted in terms of both shortening rate and geometry of the MHT. It is well known that the formulations linking surface displacements with fault geometries at depth are nonlinear [e.g., *Okada*, 1985; *Singh and Rani*, 1993]. To solve this nonlinear system, data inversion is performed using a Monte Carlo method to pseudorandomly generate a large collection of models according to the posterior probability distribution [*Mosegaard and Tarantola*, 1995]. A more detailed description of this method is provided in the supporting information.

The geometry of the MHT is defined by the coordinates of six breakpoints (a–f) (Table S3) that allow to model of a complex ramp-flat system (Figure 3). Assuming that the depth of the MHT increases northward, these coordinates are treated as dependent parameters. Furthermore, available geological and geophysical data along our study profile are used as a priori knowledge about these coordinates. This includes (1) the location of the MFT at the surface (emergence of the MHT) with a maximum dip angle of 60° [*Long et al*., 2011], (2) a subhorizontal section at a depth of 10–15 km [*Bhattacharyya and Mitra*, 2009; *Acton et al*., 2011; *Long et al*., 2011; *Tobgay et al*., 2012], (3) a maximum dip angle of 40° for crustal ramp(s) as imaged by seismic experiments in Garhwal, Nepal, and Sikkim [*Nábělek et al*., 2009; *Acton et al*., 2011; *Caldwell et al*., 2013], and (4) a depth of approximately 40 km of the southernmost point imaged beneath southern Tibet from the INDEPTH experiment [*Hauck et al*., 1998]. Because they give contrasting results, geometries obtained by *Robert et al*. [2011] and *Coutand et al*. [2014] are not used a priori but a posteriori for comparison. We assume a constant shortening rate of 15 to 18 mm/yr consistent with the convergence rate estimated across western Bhutan from GPS observations [*Vernant et al*., 2014].

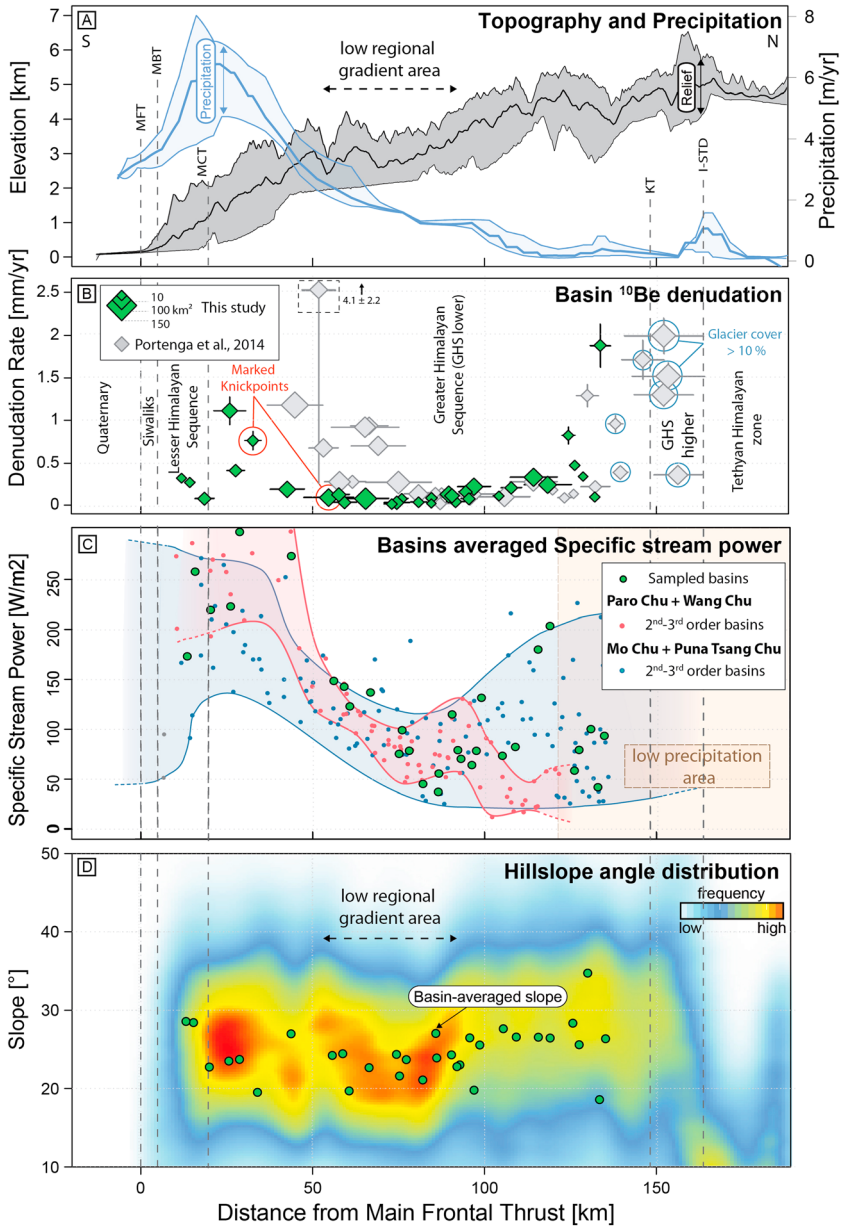

Figure 2. Swath profile (20 km wide) showing the distribution of rainfall, denudation rates, and several topographic parameters across the range (see Figure 1 for location). (a) Mean topographic profile derived from Shuttle Radar Topography Mission 90 m digital elevation model (black lines: mean, maximum, and minimum). Distribution of precipitation (blue lines: mean, maximum, and minimum) from *Bookhagen and Burbank* [2010]. Vertical dashed lines show surface location of the main tectonic structures. "Low regional gradient area" corresponds to the part of the topographic profile formed by perched patches of low-relief topography described by *Grujic et al.* [2006]. (b) Basin-averaged denudation rates derived from ^{10}Be concentration in fluvial sediments. Green and grey diamonds refer to this study and to *Portenga et al.* [2014], respectively. Error bars on denudation rates are $\pm 1\sigma$. Error bars on distance along the profile correspond to the minimum and maximum latitude of each sampled catchment. Symbol size is proportional to catchment area. Large-scale lithological units are from *Grujic et al.* [2011, and references therein]. Red circles around symbols highlight two basins with pronounced knickpoints along their main river. Blue circles around symbols highlight basins with an ice cover above 10%. (c) Distribution of basin-averaged specific stream power for sampled catchments (green circles), and second- and third-order basins along the Paro Chu/Wang Chu system (red circles) and Mo Chu/Puna Tsang Chu system (blue circles), with associated envelopes. Orange area shows the northern low-precipitation area. (d) Hillslope angles frequency profile. Green circles are average hillslope angle over the sampled catchments.

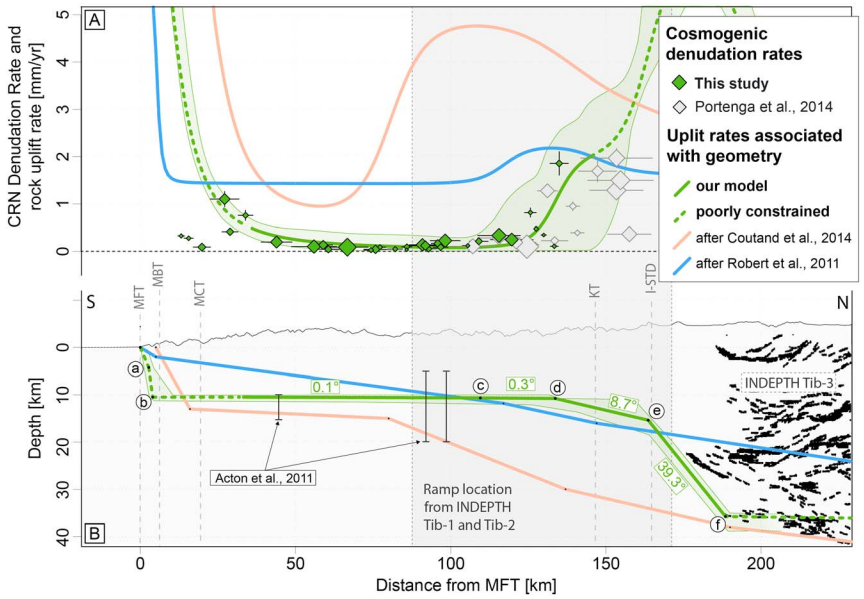

Figure 3. Denudation rates and constraints on the geometry of the MHT. (a) North-south denudation profile and calculated uplift rates. Combined denudation data set (see text) is shown by green and grey diamonds, as in Figure 2. Blue and orange lines correspond to rock uplift rates inferred from MHT geometries proposed by *Robert et al.* [2011] and *Coutand et al.* [2014], respectively. Solid green line represents the rock uplift rate derived from our best fitting model. Green envelope shows rock uplift rates associated with the 20 best fitting models. (b) North-south mean topographic profile in western Bhutan and southern Tibet. Blue and orange lines are the geometries of the MHT proposed by *Robert et al.* [2011] and *Coutand et al.* [2014], respectively. Solid green line corresponds to the geometry of the MHT obtained from our modeling. Green envelope shows the geometry of the MHT associated with the 20 best fitting models. Circled letters a to f correspond to the six breakpoints used to define the geometry. Vertical black lines are MHT depth constraints from receiver function [*Acton et al.*, 2011].

Finally, a model result consists in 13 parameters that include the shortening rate as well as the depth and distance along the profile of each of the six breakpoints. The posterior probability of each model parameter is obtained from the final collection of models.

3. Denudation Data

Measured denudation rates range from 0.025 mm/yr to 2.1 mm/yr (Figure 2b and Table S1). Their spatial distribution is consistent with the previously described contrasting geomorphic domains of the Bhutan Himalayas [*Duncan et al.*, 2003; *Adams et al.*, 2013]. From south to north, three domains can be distinguished: (1) a northward decreasing denudation trend across the range front (<50 km from the MFT), (2) very low rates within the low regional gradient area described by *Duncan et al.* [2003], and (3) a strong increase toward the northern more rugged high-relief areas (>110 km from the MFT). The transition between the Bhutanese front and the low regional gradient area is associated with a significant decrease in specific stream power (low-order tributary basins and corresponding main rivers, Figures 2c and S4, respectively). One may note that this transition also corresponds to the northern limit of the high orographic precipitation area (>3 m/yr) observed in southern Bhutan [*Bookhagen and Burbank*, 2010]. The second transition, located approximately 110 km north of the MFT, is also associated with a gradual increase in specific stream power, however, less pronounced due to very low precipitation over that area.

We note that these first-order trends are affected by evident scatter and present several outliers, such as low denudation catchments at the northern and southern ends of the profile (Figure 2b) and variability in tributary catchments stream power (Figure 2c). Some of these outliers correspond to small catchments (<10 km^2) that may present systematic bias affecting the estimation of denudation [*Niemi et al.*, 2005; *Yanites et al.*, 2009] or for which the calculation of geomorphic parameters based on river properties (steepness index or stream power) is strongly affected by the limited length of the fluvial network. We also note (1) the presence of major knickpoints within two catchments and (2) a significant percentage of glacier cover for some of the basins studied by *Portenga et al.* [2014], at the northern end of the profile

(>140 km from MFT). Despite an unavoidable amount of natural variability in the signal, we are confident in the robustness of these increasing denudation trends at both ends of our profile. Indeed, the lowest rates observed at these locations are in average higher than the lowest rates in the central part. We also note that the rapid increase in denudation rate northward is actually the development of a slower but unambiguous rise in denudation rate starting at approximately 100 km north of the MFT.

Denudation rates generally increase with the main geomorphic metrics associated with the intensity of hillslope and river erosion processes (Figure S3). Despite the existence of outliers and significant dispersion over the first-order trends, our data set appears to follow previously reported relationships, such as a power law between denudation rate and normalized steepness index and a nonlinear asymptotic evolution of denudation rate with hillslope angles [e.g., *Ouimet et al*., 2009].

4. Discussion

4.1. Spatial Pattern of Denudation

It should be emphasized that the central and northern parts of our profile overlap with the data set of *Portenga et al*. [2014] and display a similar pattern with a rapid northward increase in denudation rates. However, the southern part of our profile was sampled along the Paro Chu and the Wang Chu, whereas *Portenga et al*. [2014] focused on the Puna Tsang Chu (Figure 1). Both data sets display a significant southward increase in denudation rates exceeding 1 mm/yr but with an offset of approximately 20 km in the location of the transition. This spatial shift in the denudation patterns is consistent with the respective positions of the major knickzones along the sampled rivers (Figure S4).

The location of the denudation transition farther north along the Puna Tsang Chu may be caused by a wider valley that could allow for a deeper penetration of moisture into the range. However, available precipitation data do not show any northward deflection of the intense precipitation area that runs along the southern front of the range [*Bookhagen and Burbank*, 2010].

Several authors have proposed that the low regional gradient area may be a remnant topography (Figure S2b) [*Grujic et al*., 2006; *Adams et al*., 2013]. The climatic or tectonic origin of the associated uplift is still debated, but we note that the correspondence between the relative offsets of the knickzones along the Wang Chu and the Puna Tsang Chu and the two denudation trends is consistent with this hypothesis. These offsets could be due to a difference in the northward propagation rates of the knickzones into the low regional gradient area due to the differences in catchments size of the two rivers.

Hereinafter we combine our denudation rates with those obtained by *Portenga et al*. [2014] between the latitude of Punakha and the Bhutanese northern border. This provides an approximately 150 km long profile across western Bhutan from the range front to the northernmost high relief. Denudation in the southern part of the profile might be affected by transient landscape evolution. On the other hand, we interpret the denudation rate increase in the northern part as the result of differential rock uplift of the high range with respect to the low regional gradient area.

The first-order distinction between the three geomorphic domains along our profile is rather clear in the evolution of the pattern of denudation and specific stream power. In contrast, there are discrepancies in the respective evolution of these parameters at shorter wavelengths. As explained in section 3, the existence of natural variability in these rapidly eroding landscapes or systematic biases in the estimation of denudation rates and geomorphic metrics indices can account for some of these discrepancies. We should also keep in mind that cosmogenic nuclides concentrations are primarily reflecting hillslope denudation, whereas specific stream power or normalized steepness index are river incision proxies. As a consequence, any comparison between these parameters will be affected either by the degree of coupling between channels and hillslopes or by the time scales at which these catchments respond to climatic or tectonic perturbations [*Willenbring et al*., 2013].

4.2. Constraints on the Geometry of the MHT

We perform a joint inversion of denudation rates [this study and *Portenga et al*., 2014], GPS measurements [*Vernant et al*., 2014], and Holocene uplift rates at the front [*Berthet et al*., 2014]. As previously mentioned, our analysis is based on the assumption that denudation rates can be used as a proxy for rock uplift and that their distribution provides semiquantitative insights into the spatial variation of relative uplift rates

across the range. While some parts of the fluvial network in southern Bhutan present transient features, we are confident that the observed northward increase in denudation rates is a consequence of a local increase in rock uplift, which may be associated with a concomitant change in the geometry of the MHT. Such working hypothesis is substantiated by previous studies in central Nepal and Garwhal Himalayas where strikingly similar evolutions of denudation across the range were interpreted as a direct consequence of a ramp-flat transition along the MHT [*Godard et al*., 2014; *Scherler et al*., 2014]. Even though our inversion is based on the whole data set, we want to stress that our primary focus is to constrain the location of the ramp-flat transition associated with this particular change in denudation.

Based on a collection of 10^7 model runs, our results are in agreement with this ramp-flat system hypothesis (Figure 3). The 20 best fitting models suggest a basal décollement at a depth of approximately 10 km dipping north at only approximately 1° beneath the low regional gradient zone before connecting to a midcrustal ramp approximately at 27°30′N. This shallow dip is controlled by the very slow denudation in the central part of the transect, whereas the depth is poorly constrained by the inversion and mostly depends on a priori knowledge [*Bhattacharyya and Mitra*, 2009; *Acton et al*., 2011; *Long et al*., 2011; *Tobgay et al*., 2012]. Concerning the dip angle, our results are consistent with geophysical studies showing a subhorizontal MHT [e.g., *Nábělek et al*., 2009; *Acton et al*., 2011; *Caldwell et al*., 2013]. Conversely, when compared with these previous investigations, the width of approximately 130 km for the flat portion of the MHT is more surprising and is the main result of our study. In the Garhwal, Nepal, and Sikkim Himalayas, the location of the midcrustal flat-ramp transition is now well established at a distance of 80–100 km north of the MFT. Here we infer a transition approximately 130 km north of the MFT below the northernmost part of Bhutan.

It is important to note that our modeling is based on the assumption of topographic steady state, which is probably not valid in the southern part of the range. Under such assumption the low denudation rates in the central part of our profile are implying a very flat décollement. The low regional gradient areas are probably still out of equilibrium with the southern base level and could be undergoing surface uplift, which would require a slightly steeper flat. This does not affect the main finding of our study which is the location of the flat-ramp transition constrained by the sharp northward denudation increase.

Additionally, our modeling constrains other features of the MHT, but with a lesser degree of confidence than the location of this flat-ramp transition. In the south ($<$50 km from the MFT), our best fitting models suggest a steep frontal ramp (50–60°) connected to the basal décollement. However, this geometry should be taken with caution as the lack of denudation data near the front leads to three different models for the horizontal distance of points a and b (Figure S6). Assuming deformation by fault-bend folding, the steepest angle obtained by *Lavé and Avouac* [2000] for the MFT in central Nepal ranges from 30° to 50°. Following a similar approach, the bedding dip angles reported by *Long et al*. [2011] and *Hirschmiller et al*. [2014] at the intersection between our profile and the morphological front can be interpreted as local dips of 40–50°. Concerning the shortening rate, we obtain a value of 15.4 mm/yr. The lower edge of the interseismic locked zone is 80–120 km north of the MFT in agreement with previous results [*Vernant et al*., 2014]. However, this model is nonunique and a trade-off exists between the estimated slip rate and the depth of the subhorizontal décollement (Figure S5).

The geometry of the MHT across western Bhutan has also been investigated from the inversion of thermochronologic data [*Robert et al*., 2011; *Coutand et al*., 2014]. Forward modeling using MHT geometries from these two studies is not consistent with the combined denudation data we present here (Figure 3). A MHT geometry with a constant dip angle as proposed by *Robert et al*. [2011] involves a constant uplift rate that cannot explain the variations of denudation. Furthermore, the location of the midcrustal ramp proposed by *Coutand et al*. [2014] and mostly inferred from seismic images obtained in the Yadong-Gulu rift is not in agreement with the rapid northward denudation rate increase at approximately 110 km from the MFT.

Several explanations can be proposed for these discrepancies. First, there is obviously a significant difference in the time scales of integration of the tectonic and geomorphic processes by the two data sets used. Thermochronological data record exhumation pathways over several Ma, a time span that might encompass significant transient events such as surface uplift of the low regional gradient area or duplexing in the Lesser Himalayan sequence. Hence, part of the difference in inferred geometries could result from some unsteadiness in topographic evolution and/or tectonic processes. More importantly, we

note that in the inversion of the western Bhutan data by *Coutand et al.* [2014], the position of the ramp-flat transition is fixed a priori, based on geophysical imagery of the MHT along the INDEPTH profile in the Yadong-Gulu rift. Significant segmentation of the MHT exists along the Himalayan Arc in this area, and important changes in its geometry are likely to occur across the 40–70 km that separate these seismic profiles from our denudation profile in western Bhutan [*Hauck et al.*, 1998; *Kellett and Grujic*, 2012]. Despite the transient evolution affecting the southern part of the range, the first-order denudation rate increase observed in the northern part of our transect supports the idea of a major steepening of the MHT at that location, which is significantly farther north than other flat-ramp transitions elsewhere in the Himalayas.

5. Conclusions

We present a new data set of 32 denudation rates derived from ^{10}Be concentrations in river sediments across western Bhutan. The spatial distribution is consistent with the previously documented contrasting geomorphic domains of the Bhutan Himalayas: the High Himalayas and the Himalayan front are characterized by high denudation rates (up to approximately 2 mm/yr) with significantly lower values in between ($<$0.25 mm/yr).

This pattern of denudation can be explained by a tectonic model that includes a steep crustal ramp for the MHT fault below the northernmost relief, at approximately 130 km from the MFT. The inferred location of the ramp-flat transition strongly contrasts with geometries proposed for the MHT elsewhere along the Himalayan Arc, which has implications for its seismogenic behavior in Bhutan. This extended décollement could have the potential to generate larger earthquakes than previously expected along this section of the Himalayan Arc.

Although we consider this proposition on the ramp location to be a robust feature of our data set and associated modeling, further geophysical and geomorphic observations are now needed to better constrain the geometry of other parts of the MHT, such as the décollement depth, the dip angle of the MFT, and the geometry of the steeper segments of the MHT. Thus, additional geophysical surveys as well as geomorphic observations are now needed to address these issues.

Acknowledgments

This project is funded by the French Agence Nationale de la Recherche (ANR-13-BS06-0006-01), the CNES/ISIS program, and the CNES/TOSCA program. RLM PhD is supported by a fellowship from the French Ministry for Higher Education and Research. We would like to thank all people helping for the fieldwork in Bhutan and particularly our drivers Phajo Kinley and Tsheten from the Department of Geology and Mines. We thank also Douglas Burbank, Djordje Grujic, and an anonymous reviewer for their helpful and constructive comments. The data from this study are available in the supporting information, Tables S1–S3.

The Editor thanks Djordje Grujic for their assistance in evaluating this paper.

References

Acton, C. E., K. Priestley, S. Mitra, and V. K. Gaur (2011), Crustal structure of the Darjeeling–Sikkim Himalaya and southern Tibet, *Geophys. J. Int.*, *184*(2), 829–852.

Adams, B., K. V. Hodges, M. C. van Soest, and K. X. Whipple (2013), Evidence for Pliocene-Quaternary normal faulting in the hinterland of the Bhutan Himalaya, *Lithosphere*, *5*(4), 438–449, doi:10.1130/L277.1.

Ader, T., et al. (2012), Convergence rate across the Nepal Himalaya and interseismic coupling on the Main Himalayan Thrust: Implications for seismic hazard, *J. Geophys. Res.*, *117*, B04403, doi:10.1029/2011JB009071.

Alsdorf, D., L. Brown, K. D. Nelson, Y. Makovsky, S. Klemperer, and W. Zhao (1998a), Crustal deformation of the Lhasa terrane, Tibet plateau from Project INDEPTH deep seismic reflection profiles, *Tectonics*, *17*(4), 501–519, doi:10.1029/98TC01315.

Alsdorf, D., et al. (1998b), INDEPTH (International Deep Profiling of Tibet and the Himalaya) multichannel seismic reflection data: Description and availability, *J. Geophys. Res.*, *103*(B11), 26,993–26,999, doi:10.1029/98JB01078.

Berthet, T., J. F. Ritz, M. Ferry, P. Pelgay, R. Cattin, D. Drukpa, R. Braucher, and G. Hetényi (2014), Active tectonics in eastern Himalaya: New constraints from the first morphotectonic study in southern Bhutan, *Geology*, *42*(5), 427–430.

Bhattacharyya, K., and G. Mitra (2009), A new kinematic evolutionary model for the growth of a duplex—An example from the Rangit duplex, Sikkim Himalaya, India, *Gondwana Res.*, *16*(3), 697–715.

Bollinger, L., S. N. Sapkota, P. Tapponnier, Y. Klinger, M. Rizza, J. Van der Woerd, D. R. Tiwari, R. Pandey, A. Bitri, and S. Bes de Berc (2014), Estimating the return times of great Himalayan earthquakes in eastern Nepal: Evidence from the Patu and Bardibas strands of the Main Frontal Thrust, *J. Geophys. Res. Solid Earth*, *119*, 7123–7163, doi:10.1002/2014JB010970.

Bookhagen, B., and D. W. Burbank (2010), Toward a complete Himalayan hydrological budget: Spatiotemporal distribution of snowmelt and rainfall and their impact on river discharge, *J. Geophys. Res.*, *115*, F03019, doi:10.1029/2009JF001426.

Brown, E. T., R. F. Stallard, M. C. Larsen, and G. M. Raisbeck (1995), Denudation rates determined from the accumulation of in situ-produced ^{10}Be in the Luquillo Experimental Forest, Puerto Rico, *Earth Planet. Sci. Lett.*, *129*, 193–202.

Burgess, W. P., A. Yin, C. S. Dubey, Z. K. Shen, and T. K. Kelty (2012), Holocene shortening across the Main Frontal Thrust zone in the eastern Himalaya, *Earth Planet. Sci. Lett.*, *357*, 152–167.

Caldwell, W. B., S. L. Klemperer, J. F. Lawrence, S. S. Rai, and Ashish (2013), Characterizing the Main Himalayan Thrust in the Garhwal Himalaya, India with receiver function CCP stacking, *Earth Planet. Sci. Lett.*, *367*, 15–27, doi:10.1016/j.epsl.2013.02.009.

Cattin, R., and J. P. Avouac (2000), Modeling mountain building and the seismic cycle in the Himalaya of Nepal, *J. Geophys. Res.*, *105*, 13,389–13,407, doi:10.1029/2000JB900032.

Coutand, I., D. M. Whipp Jr., D. Grujic, M. Bernet, G. Fellin, B. Bookhagen, K. R. Landry, S. K. Ghalley, and C. Duncan (2014), Geometry and kinematics of the Main Himalayan Thrust and Neogene crustal exhumation in the Bhutanese Himalaya derived from inversion of multithermochronologic data, *J. Geophys. Res. Solid Earth*, *119*, 1446–1481, doi:10.1002/2013JB010891.

Cyr, A. J., D. E. Granger, V. Olivetti, and P. Molin (2010), Quantifying rock uplift rates using channel steepness and cosmogenic nuclide-determined erosion rates: Examples from northern and southern Italy, *Lithosphere*, *2*(3), 188–198, doi:10.1130/L96.1.

Duncan, C., J. Masek, and E. Fielding (2003), How steep are the Himalaya? Characteristics and implications of along-strike topographic variations, *Geology*, *31*(1), 75–78, doi:10.1130/0091-7613(2003)031.

Gansser, A. (1964), *Geology of the Himalayas*, Wiley Interscience, London.

Godard, V., D. W. Burbank, D. L. Bourlès, B. Bookhagen, and R. Braucher (2012), Impact of glacial erosion on ^{10}Be concentrations in fluvial sediments of the Marsyandi catchment, central Nepal, *J. Geophys. Res.*, *117*, F03013, doi:10.1029/2011JF002230.
Godard, V., D. L. Bourlès, F. Spinabella, D. W. Burbank, B. Bookhagen, G. B. Fisher, A. Moulin, and L. Léanni (2014), Dominance of tectonics over climate in Himalayan denudation, *Geology*, *42*, 243–246.
Grujic, D., I. Coutand, B. Bookhagen, S. Bonnet, A. Blythe, and C. Duncan (2006), Climatic forcing of erosion, landscape, and tectonics in the Bhutan Himalayas, *Geology*, *34*(10), 801–804.
Grujic, D., C. J. Warren, and J. L. Wooden (2011), Rapid synconvergent exhumation of Miocene-aged lower orogenic crust in the eastern Himalaya, *Lithosphere*, *3*(5), 346–366.
Gudmundsdottir, M. H., K. Blisniuk, Y. Ebert, N. M. Levine, D. H. Rood, A. Wilson, and G. E. Hilley (2013), Restraining bend tectonics in the Santa Cruz Mountains, California, imaged using ^{10}Be concentrations in river sands, *Geology*, *41*(8), 843–846, doi:10.1130/G33970.1.
Hammer, P., T. Berthet, G. Hetényi, R. Cattin, D. Drukpa, J. Chophel, S. Lechmann, N. Le Moigne, C. Champollion, and E. Doerflinger (2013), Flexure of the India plate underneath the Bhutan Himalaya, *Geophys. Res. Lett.*, *40*, 4225–4230, doi:10.1002/grl.50793.
Hauck, M. L., K. D. Nelson, L. D. Brown, W. Zhao, and A. R. Ross (1998), Crustal structure of the Himalayan orogen at ~90 east longitude from Project INDEPTH deep reflection profiles, *Tectonics*, *17*(4), 481–500, doi:10.1029/98TC01314.
Hetényi, G., J. Singer, E. Kissling, T. Diehl, J. Chophel, A. Burtin, S. Löw, and D. Drukpa (2014), Crustal structure, seismicity and landslide activity in Bhutan—Preliminary results from a temporary seismological network, Abstract Book, 29th Himalaya-Karakoram-Tibet Workshop, p. 65, edited by C. Montomoli et al., pp. 178, Lucca, Italy, Museo Regionale di Scienze Naturali, Torino, 2-4 Sept.
Hirschmiller, J., D. Grujic, B. Bookhagen, I. Coutand, P. Huyghe, J. L. Mugnier, and T. Ojha (2014), What controls the growth of the Himalayan foreland fold-and-thrust belt?, *Geology*, *42*(3), 247–250.
Kellett, D. A., and D. Grujic (2012), New insight into the South Tibetan detachment system: Not a single progressive deformation, *Tectonics*, *31*, TC2007, doi:10.1029/2011TC002957.
Kellett, D. A., D. Grujic, and S. Erdmann (2009), Miocene structural reorganization of the South Tibetan detachment, eastern Himalaya: Implications for continental collision, *Lithosphere*, *1*(5), 259–281.
Lavé, J., and J.-P. Avouac (2000), Active folding of fluvial terraces across the Siwaliks Hills, Himalayas of central Nepal, *J. Geophys. Res.*, *105*, 5735–5770, doi:10.1029/1999JB900292.
Lavé, J., and J.-P. Avouac (2001), Fluvial incision and tectonic uplift across the Himalayas of central Nepal, *J. Geophys. Res.*, *106*, 26,561–26,591, doi:10.1029/2001JB000359.
Long, S., N. McQuarrie, T. Tobgay, D. Grujic, and L. Hollister (2011), Geologic map of Bhutan, *J. Maps*, *7*, 184–192, doi:10.4113/jom.2011.1159.
Lupker, M., P.-H. Blard, J. Lavé, C. France-Lanord, L. Leanni, N. Puchol, J. Charreau, and D. Bourlès (2012), ^{10}Be-derived Himalayan denudation rates and sediment budgets in the Ganga basin, *Earth Planet. Sci. Lett.*, *333–334*, 146–156.
Mosegaard, K., and A. Tarantola (1995), Monte Carlo sampling of solutions to inverse problems, *J. Geophys. Res.*, *100*(B7), 12,431–12,447, doi:10.1029/94JB03097.
Nábělek, J., G. Hetényi, J. Vergne, S. Sapkota, B. Kafle, M. Jiang, H. Su, J. Chen, B. S. Huang, and the Hi-CLIMB Team (2009), Underplating in the Himalaya-Tibet collision zone revealed by the Hi-CLIMB experiment, *Science*, *325*(5946), 1371–1374, doi:10.1126/science.1167719.
Niemi, N. A., M. Oskin, D. W. Burbank, A. M. Heimsath, and E. J. Gabet (2005), Effects of bedrock landslides on cosmogenically determined erosion rates, *Earth Planet. Sci. Lett.*, *237*(3–4), 480–498, doi:10.1016/j.epsl.2005.07.009.
Norton, K. P., F. von Blanckenburg, and P. W. Kubik (2010), Cosmogenic nuclide-derived rates of diffusive and episodic erosion in the glacially sculpted upper Rhone Valley, Swiss Alps, *Earth Surf. Processes Landforms*, *35*(6), 651–662.
Okada, Y. (1985), Surface deformation due to shear and tensile faults in a half-space, *Bull. Seismol. Soc. Am.*, *75*(4), 1135–1154.
Ouimet, W. B., K. X. Whipple, and D. E. Granger (2009), Beyond threshold hillslopes: Channel adjustment to base-level fall in tectonically active mountain ranges, *Geology*, *37*(7), 579–582, doi:10.1130/G30013A.1.
Portenga, E. W., P. R. Bierman, C. Duncan, L. B. Corbett, N. M. Kehrwald, and D. H. Rood (2014), Erosion rates of the Bhutanese Himalaya determined using in situ-produced ^{10}Be, *Geomorphology*, doi:10.1016/j.geomorph.2014.09.027.
Replumaz, A., and P. Tapponnier (2003), Reconstruction of the deformed collision zone between India and Asia by backward motion of lithospheric blocks, *J. Geophys. Res.*, *108*(B6, 2285), doi:10.1029/2001JB000661.
Robert, X., P. Van Der Beek, J. Braun, C. Perry, and J.-L. Mugnier (2011), Control of detachment geometry on lateral variations in exhumation rates in the Himalaya: Insights from low-temperature thermochronology and numerical modeling, *J. Geophys. Res.*, *116*, B05202, doi:10.1029/2010JB007893.
Scherler, D., B. Bookhagen, and M. R. Strecker (2014), Tectonic control on ^{10}Be-derived erosion rates in the Garhwal Himalaya, India, *J. Geophys. Res. Earth Surf.*, *119*, 82–105.
Schulte-Pelkum, V., G. Monsalve, A. Sheehan, M. R. Pandey, S. Sapkota, R. Bilham, and F. Wu (2005), Imaging the Indian subcontinent beneath the Himalaya, *Nature*, *435*, 1222–1225.
Singh, S. J., and S. Rani (1993), Crustal deformation associated with two-dimensional thrust faulting, *J. Phys. Earth*, *41*, 87–101.
Tobgay, T., N. McQuarrie, S. Long, M. J. Kohn, and S. L. Corrie (2012), The age and rate of displacement along the Main Central Thrust in the western Bhutan Himalaya, *Earth Planet. Sci. Lett.*, *319*, 146–158.
Vance, D., M. Bickle, S. Ivy-Ochs, and P. W. Kubik (2003), Erosion and exhumation in the Himalaya from cosmogenic isotope inventories of river sediment, *Earth Planet. Sci. Lett.*, *206*(3–4), 273–288.
Vernant, P., R. Bilham, W. Szeliga, D. Drukpa, S. Kalita, A. K. Bhattacharyya, V. K. Gaur, P. Pelgay, R. Cattin, and T. Berthet (2014), Clockwise rotation of the Brahmaputra Valley relative to India: Tectonic convergence in the eastern Himalaya, Naga Hills and Shillong Plateau, *J. Geophys. Res. Solid Earth*, *119*, 6558–6571, doi:10.1002/2014JB011196.
Von Blanckenburg, F. (2005), The control mechanisms of erosion and weathering at basin scale from cosmogenic nuclides in river sediment, *Earth Planet. Sci. Lett.*, *237*(3–4), 462–479.
Willenbring, J. K., N. M. Gasparini, B. T. Crosby, and G. Brocard (2013), What does a mean mean? The temporal evolution of detrital cosmogenic denudation rates in a transient landscape, *Geology*, *41*(12), 1215–1218.
Wittmann, H., F. von Blanckenburg, T. Kruesmann, K. P. Norton, and P. W. Kubik (2007), Relation between rock uplift and denudation from cosmogenic nuclides in river sediment in the Central Alps of Switzerland, *J. Geophys. Res.*, *112*, F04010, doi:10.1029/2006JF000729.
Wobus, C., A. Heimsath, K. Whipple, and K. Hodges (2005), Active out-of-sequence thrust faulting in the central Nepalese Himalaya, *Nature*, *434*, 1008–1011.
Yanites, B. J., G. E. Tucker, and R. S. Anderson (2009), Numerical and analytical models of cosmogenic radionuclide dynamics in landslide-dominated drainage basins, *J. Geophys. Res.*, *114*, F01007, doi:10.1029/2008JF001088.